Phase diagrams of $Ba(Fe_{1-x}M_x)_2As_2$ single crystals (M=Rh and Pd)

N. Ni, A. Thaler, A. Kracher, J. Q. Yan, S. L. Bud'ko, and P. C. Canfield
Ames Laboratory and Department of Physics and Astronomy, Iowa State University, Ames, Iowa 50011, USA
(Received 21 May 2009; revised manuscript received 17 June 2009; published 17 July 2009)

Single crystalline $Ba(Fe_{1-x}M_x)_2As_2$ (M=Rh,Pd) series have been grown and characterized by structural, thermodynamic, and transport measurements. These measurements show that the structural/magnetic phase transitions, found in pure $BaFe_2As_2$ at 134 K, are suppressed monotonically by the doping and that superconductivity can be stabilized over a domelike region. Temperature-composition ($T-x$) phase diagrams based on electrical transport and magnetization measurements are constructed and compared to those of the $Ba(Fe_{1-x}M_x)_2As_2$ (M=Co,Ni) series. Despite the generic difference between 3d and 4d shells and the specific, conspicuous differences in the changes to the unit cell parameters, the effects of Rh doping are exceptionally similar to the effects of Co doping and the effects of Pd doping are exceptionally similar to the effects of Ni doping. These data show that whereas the structural/antiferromagnetic phase-transition temperatures can be parameterized by x and the superconducting transition temperature can be parameterized by some combination of x and e, the number of extra electrons associated with the M doping, the transition temperatures of 3d- and 4d-doped $BaFe_2As_2$ cannot be simply parameterized by the changes in the unit-cell dimensions or their ratios.

DOI: 10.1103/PhysRevB.80.024511 PACS number(s): 74.10.+v, 74.62.Dh, 74.70.Dd, 75.30.Kz

I. INTRODUCTION

The discovery of superconductivity in F-doped LaFeAsO[1] and K-doped $BaFe_2As_2$ (Ref. 2) compounds in the first half of 2008 has led to extensive experimental interest; T_c has risen as high as 56 K for F doped RFeAsO systems[3] and as high as 38 K in K and Na doped $(AE)Fe_2As_2$ systems (AE: Ba, Sr, Ca).[2] Soon after, superconductivity was also found in Co and Ni doped $(AE)Fe_2As_2$ (Refs. 4 and 5) and RFeAsO.[6] Recently, superconductivity was also found in 4d and 5d transition metal electron doped $SrFe_2As_2$.[7–10] Although electron doped $(AE)Fe_2As_2$ systems have lower T_c values ($\sim$24 K),[11–14] intensive studies have been made on them because doping is more homogeneous in these systems and the single crystals can be easily grown and reproduced. For example, several studies of $Ba(Fe_{1-x}Co_x)_2As_2$ system have resulted in remarkably similar data and conclusions.[11–14] In order to compare the effects of 3d and 4d electron doping in $BaFe_2As_2$, and thus try to understand the conditions for the appearance of superconductivity in these systems, carefully constructed $T-x$ phase diagrams are needed. Elemental analysis, preferably of single crystal samples, should be used to determine the actual percentage of the dopant inside the lattice rather than the nominal doping level. Recently such a detailed study was made for Co doped $BaFe_2As_2$,[11–16] as well as for Ni, Cu, and Cu/Co mixes.[17] These data on 3d, electron doped $BaFe_2As_2$ raised the question of whether the number of impurities, the band filling, and/or the unit-cell dimensions were the physically salient variables. For this paper, $Ba(Fe_{1-x}M_x)_2As_2$ (M=Rh,Pd) series have been studied by the electrical transport, magnetization, specific heat, and wavelength dispersive spectroscopy. We find that the $T-x$ phase diagrams for Co and Rh doping are virtually identical, as are the phase diagrams for Ni and Pd doping. By analysis of the relative changes in the unit-cell parameters we can conclude that whereas x and e can still successfully be used to parameterize the structural/magnetic and superconducting phase transitions in the $Ba(Fe_{1-x}M_x)_2As_2$ systems, changes in the unit-cell parameters, or their ratios, no longer can.

II. EXPERIMENTAL METHODS

Single crystals of $Ba(Fe_{1-x}M_x)_2As_2$ (M=Rh,Pd) were grown out of self flux using conventional high-temperature solution growth techniques.[11,18] FeAs, RhAs and PdAs powder were synthesized in the same manner as in Ref. 11. Small Ba chunks, FeAs/RhAs or FeAs/PdAs powder were mixed together according to the ratio Ba:MAs=1:4. The mixture was placed into an alumina crucible with a second "catch" crucible containing quartz wool placed on top. Both crucibles were sealed in a quartz tube under a 1/3 partial atmosphere of Ar gas. The sealed quartz tube was heated up to 1180 °C over 12 h, held at 1180 °C for 5 h, and then cooled to 1050 °C over 36 h. Once the furnace reached 1050 °C, the excess FeAs/RhAs or FeAs/PdAs liquid was decanted from the plate like single crystals.

Powder x-ray diffraction measurements, with a Si standard, were performed using a Rigaku Miniflex diffractometer with Cu K_α radiation at room temperature. Diffraction patterns were taken on ground single crystals from each batch. No detectable impurities were found in these compounds. The unit cell parameters were refined by "UnitCell" software. Error bars were taken as twice the standard deviation, σ, which was obtained from the refinements by the "Unitcell" software. Elemental analysis of the samples was performed using wavelength dispersive x-ray spectroscopy (WDS) in the electron probe microanalyzer of a JEOL JXA-8200 electron microprobe. Magnetization and temperature-dependent ac electrical resistance data (f=16 Hz, I=3 mA) were collected in a Quantum Design (QD) Magnetic Property Measurement System (MPMS) using LR700 resistance bridge for the latter. Electrical contact was made to the sample using Epotek H20E silver epoxy to attach Pt wires in a four-probe configuration. Heat-capacity data were collected

TABLE I. The WDS data for $Ba(Fe_{1-x}Rh_x)_2As_2$ and $Ba(Fe_{1-x}Pd_x)_2As_2$. N is the number of locations measured in one batch, x_{ave} is the average x value measured in one batch, 2σ is two times the standard deviation of the N values measured.

				$Ba(Fe_{1-x}Rh_x)_2As_2$				
N	16	16	18	15	20	34	33	20
x_{ave}	0.012	0.026	0.039	0.057	0.076	0.096	0.131	0.171
2σ	0.001	0.001	0.002	0.003	0.004	0.006	0.005	0.002
				$Ba(Fe_{1-x}Pd_x)_2As_2$				
N	18	8	52	6	6	12	14	52
x_{ave}	0.012	0.021	0.027	0.030	0.043	0.053	0.067	0.077
2σ	0.001	0.002	0.003	0.002	0.001	0.002	0.002	0.005

using a QD Physical Property Measurement System (PPMS) using the relaxation technique.

III. RESULTS

Summaries of the WDS measurement data are shown in Table I for both $Ba(Fe_{1-x}Rh_x)_2As_2$ and $Ba(Fe_{1-x}Pd_x)_2As_2$. For each batch, up to five pieces of samples were measured. The table shows the number of locations measured, the average of the x values measured at these locations, and two times the standard deviation of the x values measured on these locations, which is taken as the error bar in this paper. We can see that the 2σ error bars are $\lesssim 10\%$ of the average x values. The average x value, x_{ave}, obtained from wavelength dispersive x-ray spectroscopy (WDS) measurement will be used for all the compounds in this paper rather than nominal x. It is worth noting that separate measurements of x_{ave} on the resistivity bars gave values within the 2σ error bars for all the measured batches.

Figure 1 presents the normalized electrical resistivity data of the $Ba(Fe_{1-x}Rh_x)_2As_2$ series from base temperature, 2 to 300 K. Normalized resistivity, instead of resistivity, is plotted because of the tendency of these samples to exfoliate or partially crack.[11,19,20] The resistive anomaly at 134 K for pure $BaFe_2As_2$ is associated with the structural/magnetic phase transitions.[21] As in the case of Co, Ni and Cu substitutions,[11,17] as x is increased the temperature of the resistive anomaly is suppressed monotonically and the shape of the feature changes from a sharp decrease in pure $BaFe_2As_2$ to a broadened increase in doped samples. It is no longer detectable for $x \geq 0.057$. For $x=0.026$, superconductivity becomes detectable, with $T_c \approx 3$ K inferred from the sharp drop in the resistivity data. For $x=0.057$, superconducting temperature T_c has a maximum value of 24 K with a width $\Delta T_c \approx 0.7$ K. With even higher x, T_c is suppressed.

Figure 2 shows the M/H data for the $Ba(Fe_{1-x}Rh_x)_2As_2$ series taken at 25 Oe with H perpendicular to the crystallographic c axis. A clear diamagnetic signal can be seen in both field-cooled (FC) and zero-field-cooled (ZFC) data. Because of the low T_c values for $x=0.026$ and $x=0.131$, which are on the low- and high-x extremes of the superconductivity dome respectively, we only observe the onset of the diamagnetic signal and no large drop below the superconducting temperature is seen down to our base temperature of 2 K. However, for all the other concentrations, the large superconducting, shielding fraction and the sharp drop below T_c are consistent with the existence of bulk superconductivity. Compared to

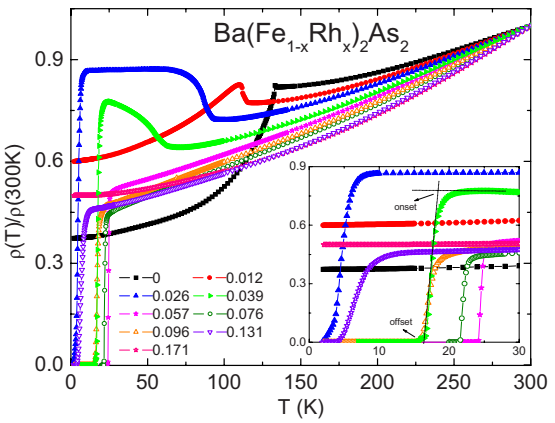

FIG. 1. (Color online) The temperature-dependent resistivity, normalized by the room temperature value, for $Ba(Fe_{1-x}Rh_x)_2As_2$. Inset: low-temperature data for $Ba(Fe_{1-x}Rh_x)_2As_2$. On- and off-set criteria for T_c are shown.

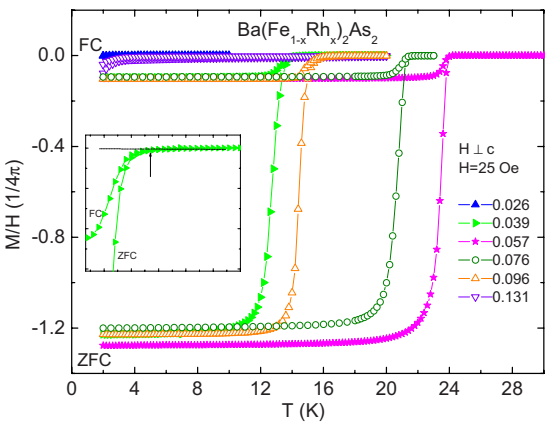

FIG. 2. (Color online) Low magnetic-field M/H for $Ba(Fe_{1-x}Rh_x)_2As_2$ series. Inset: the criterion used to infer T_c is shown for $Ba(Fe_{0.961}Rh_{0.039})_2As_2$.

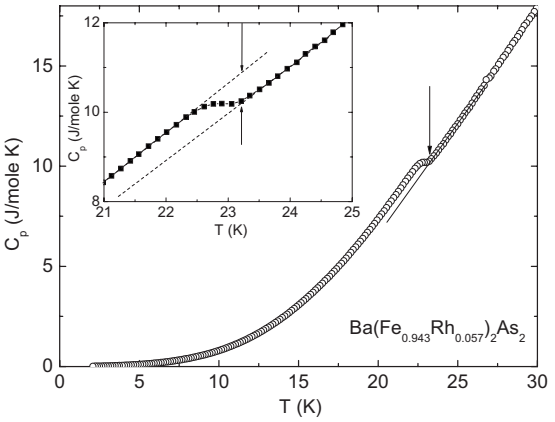

FIG. 3. Temperature-dependent heat-capacity data for $Ba(Fe_{0.943}Rh_{0.057})_2As_2$. Inset: C_p vs T near the superconducting transition with the estimated ΔC_p shown.

the low-field M/H data for $Ba(Fe_{1-x}Co_x)_2As_2$,[11] the superconducting fraction associated with the $Ba(Fe_{1-x}Rh_x)_2As_2$ series have very similar values as of $Ba(Fe_{1-x}Co_x)_2As_2$ series.

The temperature-dependent heat-capacity data for $Ba(Fe_{0.943}Rh_{0.057})_2As_2$ is shown in Fig. 3. This concentration has the maximum T_c value in this series. The heat capacity anomaly is relatively sharp and consistent with the superconducting phase transition we observed in both resistivity and low-field magnetization data. The large arrow in the inset shows the onset of superconductivity and $T_c=23.2$ K. A way to estimate ΔC_p is also shown in the inset; $\Delta C_p \approx 700$ mJ/mole K. Assuming the BCS weak coupling approximation $\Delta C_p/\gamma T_c=1.43$ and 100% superconducting volume, the γ value for $Ba(Fe_{0.943}Rh_{0.057})_2As_2$ can be estimated to be about 20 mJ/mol K^2, which is comparable to the value estimated in the same manner for $Ba(Fe_{0.943}Co_{0.074})_2As_2$.[22]

Figure 4 shows the normalized electrical resistivity data for the $Ba(Fe_{1-x}Pd_x)_2As_2$ series from base temperature, 2 to 300 K. A systematic behavior, similar to the $Ba(Fe_{1-x}Rh_x)_2As_2$ series, is seen: the temperature of the resistive anomaly associated with the structural/antiferromagnetic phase transitions is suppressed monotonically with Pd doping and the shape of the anomaly changes from a

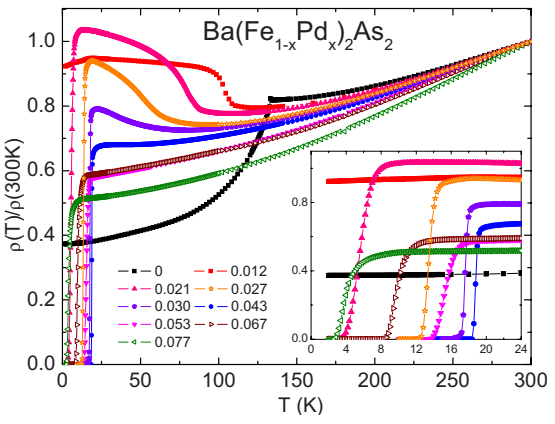

FIG. 4. (Color online) The temperature-dependent resistivity, normalized by room temperature value, for $Ba(Fe_{1-x}Pd_x)_2As_2$. Inset: low-temperature data for $Ba(Fe_{1-x}Pd_x)_2As_2$.

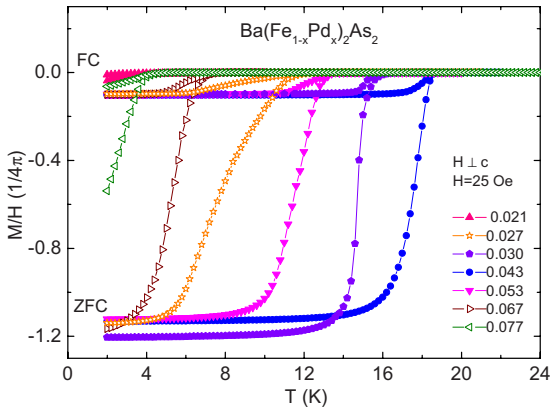

FIG. 5. (Color online) Low magnetic-field M/H for $Ba(Fe_{1-x}Rh_x)_2As_2$ series.

sharp decrease to a broadened increase in resistivity upon cooling. For $x=0.021$, the resistive anomaly can still be clearly seen and superconductivity is detected with $T_c \approx 5.7$ K. For $x=0.043$, the temperature of the resistive anomaly is further reduced and it is only inferred from a minimum in the resistivity above the superconducting transition. For $x=0.053$, the resistive anomaly is completely suppressed and T_c has its highest value of about 19 K and a width of $\Delta T_c \approx 0.6$ K. With higher x values, T_c is suppressed.

The low-field M/H data for the $Ba(Fe_{1-x}Pd_x)_2As_2$ series (FC and ZFC) are shown in Fig. 5. They were taken at 25 Oe with H perpendicular to the crystallographic c axis. The broader feature seen in the magnetization for $x=0.027$ implies a larger inhomogeneity associated with this sample. Indeed, the WDS data for $x=0.027$ does show local maximum in 2σ values. Despite the broader drop of the magnetization, the large superconducting fraction is comparable to the rest of the Pd-doped series as well as to the Co, Ni, and Rh doped $BaFe_2As_2$ results, all of which are consistent with bulk superconductivity. Again, only a small diamagnetic signal was observed at base temperature for $x=0.021$ due to the low T_c for this concentration.

Figure 6 shows the temperature-dependent heat-capacity data for $Ba(Fe_{0.957}Pd_{0.043})_2As_2$, which manifests the highest T_c value in this series. The heat-capacity anomaly at T_c can be clearly seen, although it is broader than the one found for $Ba(Fe_{0.943}Rh_{0.057})_2As_2$ (Fig. 3). The arrows show the onset of superconductivity at $T_c=18$ K and the estimated ΔC_p is shown in the inset; $\Delta C_p \approx 410$ mJ/mol K. Using the BCS weak coupling approximation $\Delta C_p/\gamma T_c=1.43$ and assuming 100% superconducting volume in this sample, γ for $Ba(Fe_{0.957}Pd_{0.043})_2As_2$ is estimated to be about 16 mJ/mol K^2.

IV. DISCUSSION

The data presented in Figs. 1–6 are summarized in the two, $T-x$, phase diagrams shown in Fig. 7. In this paper, the temperature of structural/magnetic phase transitions are inferred from the derivative of the temperature-dependent resistivity data which shows a split feature for finite values of

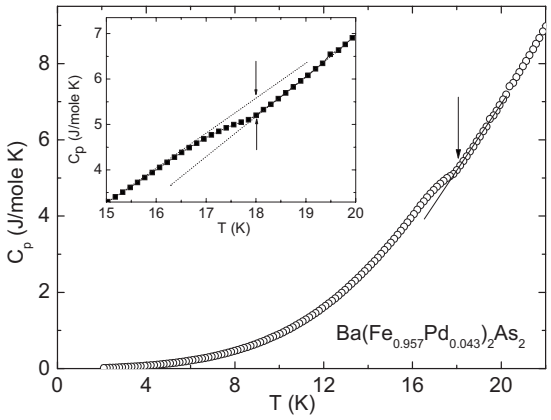

FIG. 6. Temperature-dependent heat-capacity data for $Ba(Fe_{0.957}Pd_{0.043})_2As_2$. Inset: C_p vs T near the superconducting transition with the estimated ΔC_p shown.

x.[11] The inset to Fig. 7 shows such a $d\rho/dT$ curve as well as the criteria used to determine the upper (structural) transition and the lower (antiferromagnetic) transition temperatures. As shown in Ref. 16 these criteria identify transition temperatures that agree well with the results of neutron- and x-ray diffraction measurements. On- and off-set criteria, which are shown in the inset of Fig. 1, are used to determine T_c from the resistivity data. The criterion which is shown in the inset of Fig. 2 is used to determine T_c from the magnetization data. The arrows in Fig. 3 show the criterion used to infer T_c from heat-capacity data. We can see good agreement between resistivity, magnetization, and heat-capacity measurements. So

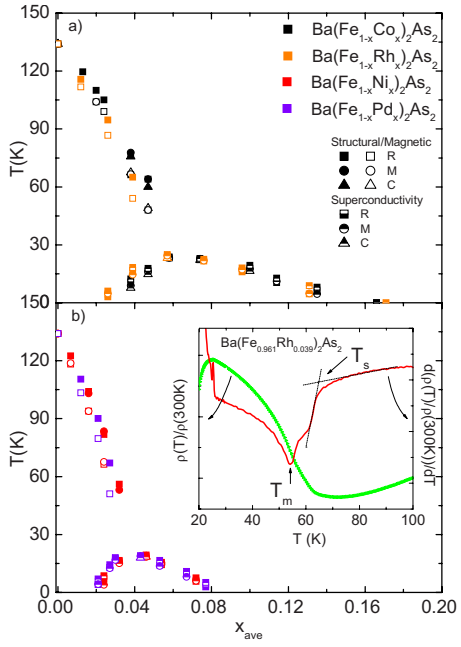

FIG. 7. (Color online) Transition temperature as a function of x. (a) $T-x$ phase diagrams of $Ba(Fe_{1-x}Rh_x)_2As_2$ and $Ba(Fe_{1-x}Co_x)_2As_2$ series. (b) Phase diagrams of $Ba(Fe_{1-x}Pd_x)_2As_2$ and $Ba(Fe_{1-x}Ni_x)_2As_2$ series. For both plots the transition temperatures were determined in a manner similar to that described in Ref. 11 and illustrated in the inset for $Ba(Fe_{0.961}Rh_{0.039})_2As_2$. Data for Co and Ni doping are taken from Refs. 11 and 17.

as to allow comparison with the isoelectronic, $3d$ electron doped $BaFe_2As_2$ compounds, data for $Ba(Fe_{1-x}M_x)_2As_2$ (M =Co,Ni) (Refs. 11 and 17) are also shown.

The upper panel presents the $T-x$ phase diagrams of Rh and Co doped $BaFe_2As_2$ and the lower panel presents the $T-x$ phase diagrams of Pd and Ni doped $BaFe_2As_2$. It can be seen in both panels that the higher-temperature structural/magnetic phase transitions are suppressed monotonically in a similar manner/rate for all series. Superconductivity is found in both tetragonal and orthorhombic phase,[11–14] and is stabilized in a domelike region for all series. Superconductivity is found over a wider range of Co or Rh doping with a maximum T_c around 24 K, and a narrower range of Ni or Pd doping with a maximum T_c around 19 K.

The complete phase diagram of Rh doped $BaFe_2As_2$ including both structural/magnetic phase transition and superconductivity shows incredible similarity as the phase diagram of Co doped $BaFe_2As_2$ and the complete phase diagram of Pd doped $BaFe_2As_2$ shows incredible similarity as the phase diagram of Ni doped $BaFe_2As_2$. For each of the pairs, the phase diagrams show exceptionally similar behavior on the rate of the suppression of structural/magnetic phase transitions, the range of superconducting domes and the maximum T_c. It is worth mentioning again that to see this, the actual x values are vital. A similar agreement between $T_c(x)$ domes for Co/Rh and Ni/Pd has been noted in $Sr(Fe_{1-x}M_x)_2As_2$.[23]

In our previous work,[17] we compared the transition temperatures as a function of x, and as a function of the number of extra conduction electrons, e, added by the dopant per Fe/M site for Co, Ni, Cu, and Co/Cu doped $BaFe_2As_2$ (for the case of Co: $e=x$, for the case of Ni: $e=2x$). We conclude that whereas the suppression of the structural/antiferromagnetic transitions was parameterized somewhat better by the number of M dopant ions (or, equivalently, changes in the c axis) the superconducting dome was parameterized by the number of electrons added by doping (or, equivalently, changes in the values of the a/c ratio), and exists over a limited range of e values (or band filling). Unfortunately we could not experimentally separate the effects of x and e from changes in c and a/c, respectively.[17] However, with current, $4d$-electron doped $BaFe_2As_2$ data, we can actually distinguish between x and e on one hand and c, a/c on the other. Figure 8 shows the unit-cell parameters normalized by the lattice parameters of pure $BaFe_2As_2$. To compare the unit-cell parameters, the data for Co or Ni doped $BaFe_2As_2$ (Refs. 11 and 17) are also plotted in Fig. 8. The lattice parameter c decreases with all dopings and the ratio of a/c increases with all dopings. But in both cases there is a clear difference between the $3d$- and $4d$-data sets. Unlike in our previous work,[17] where for $3d$-electron doping series and c can be scaled with x, and a/c can be scaled with the number of extra electron added per Fe/M site, when $4d$-electron doped $BaFe_2As_2$ data are taken into account, changes in c and a/c are no longer equivalent to x and e. This means that if we want to parameterize the effects of $3d$- and $4d$-M doping on the transitions temperatures of $Ba(Fe_{1-x}M_x)_2As_2$, whereas the upper, structural, and magnetic phase transitions can be parameterized by x and the superconducting dome can be parameterized by e, they are no longer well parameterized

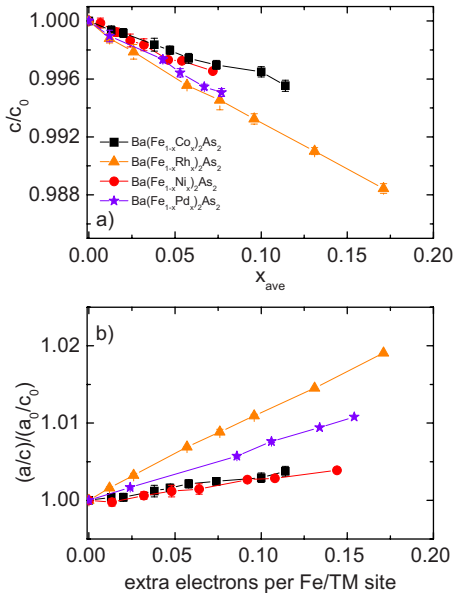

FIG. 8. (Color online) Normalized structural parameters measured at ~300 K. (a) c/c_0 as a function of transition metal doping, x and (b) $(a/c)/(a_0/c_0)$ as a function of extra conduction electrons, e. [a_0=3.9621(4) Å, c_0=13.0178(10) Å.] Data for Co and Ni doping are taken from Refs. 11 and 17.

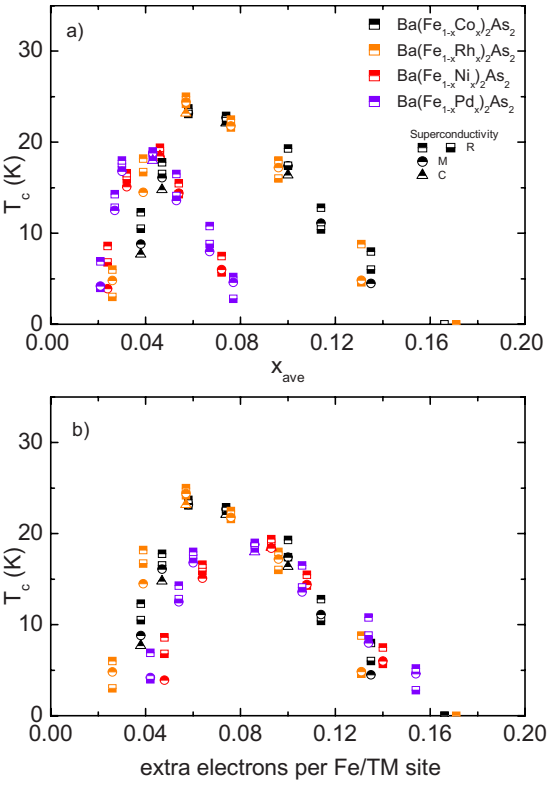

FIG. 9. (Color online) (a) Superconducting transition temperature T_c as a function of x_{ave}. (b) Superconducting transition temperature T_c as a function of extra electrons per Fe/M site. Data for Co and Ni doping are taken from Refs. 11 and 17.

by either c or a/c. As discussed in Ref. 17, it is still possible that some other parameter, such as bonding angles associated with the As position, offer better or alternate parameterization of these transition temperatures, but these are not currently known.

The parameterization scheme outlined above is based on the premise that a single parameter may be controlling the variation in the upper, structural, and magnetic transition temperatures (T_s and T_m) and a second one may be controlling the superconductivity (T_c). There is another scheme that should be discussed in the context of our growing data set: that there may be a single parameter that controls the behavior of the system when $T_s \sim T_m > T_c$ and there is another single parameter when T_s and T_m are fully suppressed. The potential appeal of this scheme can be seen in Fig. 9, where T_c is plotted as a function of e and x for comparison. As discussed above and in Ref. 17, there is excellent agreement of the T_c values when plotted as a function of e when T_s and T_m are fully suppressed. On the other hand there is arguably better agreement of the T_c values when they are plotted as a function of x for $T_s \sim T_m > T_c$. As pointed out in Ref. 17 the behavior on the $T_s \sim T_m > T_c$ side of the dome may be associated with the need to bring the upper transitions to low enough temperature so as to allow the superconductivity to turn on. The importance of reducing T_s and T_m may be associated with reducing the degree of orthorhombic splitting, the size of the ordered moment in the AF phase, and/or changing the magnetic excitation spectrum.

Given that T_s and T_m only roughly scale with x, it is worth while examining the correlation between T_s, T_m, and T_c more directly. Figure 10 plots T_c as a function of the structural, as well as the magnetic, transition temperature (given that they are split by the time superconductivity is stabilized).[11,12,15,16]

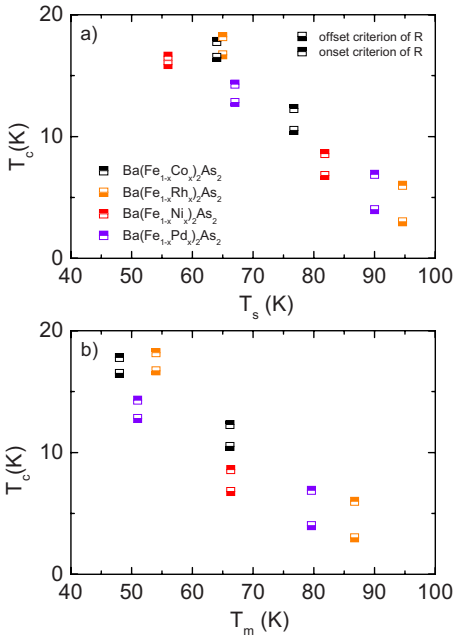

FIG. 10. (Color online) (a) Superconducting transition temperature T_c as a function of structural phase transition temperature T_s. (b) Superconducting transition temperature T_c as a function of magnetic phase transition temperature T_m. Data for Co and Ni doping are taken from Refs. 11 and 17.

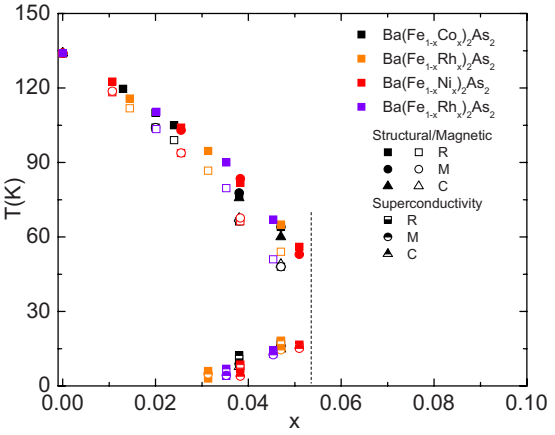

FIG. 11. (Color online) Transition temperature as a function of adjusted x. x is normalized so as to bring the interpolated values of T_s onto the transition associated with $Ba(Fe_{0.953}Co_{0.047})_2As_2$ for Co doped $BaFe_2As_2$, $x=x_{ave}$; for Rh doped $BaFe_2As_2$, $x=x_{ave}\times 0.047/0.039$; for Pd doped $BaFe_2As_2$, $x=x_{ave}\times 0.047/0.028$; for Ni doped $BaFe_2As_2$, $x=x_{ave}\times 0.047/0.03$. Data for Co and Ni doping are taken from Refs. 11 and 17.

Both plots show a clear correlation. A more graphic way of examining the correlation between T_c and T_s/T_m is to create a composite diagram for the $T_s\sim T_m>T_c$ data by adjusting the x scales for the Ni, Rh, and Pd data so as to collapse the T_s and T_m phase lines onto the Co data set. This is plotted in Fig. 11. As we can see, a clear consequence of this is to bring collapse the T_c data onto a single phase line as well.

V. CONCLUSION

Single crystalline $Ba(Fe_{1-x}M_x)_2As_2$ (M=Rh,Pd) samples have been grown and characterized by microscopic, thermodynamic, and transport measurements. $T-x$ phase diagrams were constructed for both the Rh- and Pd-doping series and, remarkably, they are virtually indistinguishable from the $T-x$ phase diagrams assembled for their $3d$-shell counterpart, Co and Ni doped, series. Given that the variations of the unit-cell parameters are distinctly different for the $3d$ and $4d$ dopants, these data clearly show that whereas the amount of dopant, x, and the change in electron count, e, do a fair job of parameterizing the structural/magnetic and superconducting phase transitions temperatures, respectively, the variation in the c-axis lattice parameter and the variation in the ratio of the a/c parameters no longer do.

Whereas the structural and magnetic phase transitions are fairly well parameterized by x and, for $T_c>T_s/T_m$, T_c is parameterized by e very well, the T_c data for $T_s\sim T_m>T_c$ appears to depend on the degree of suppression of T_s/T_m (and therefore may depend more on x than on e). The fact that the behavior of T_c in response to doping appears to change in the vicinity of the disappearance of T_s/T_m is consistent with recent studies of the $T-P$ phase diagram for $BaFe_2As_2$ (Ref. 24) as well as earlier work on K doped $BaFe_2As_2$.[25] In every case T_c appears to reach its maximum value [varying from M, to K, to P (Ref. 26) doped] when T_s and T_m are suppressed below T_c.

ACKNOWLEDGMENTS

Work at the Ames Laboratory was supported by the Department of Energy, Basic Energy Sciences under Contract No. DE-AC02-07CH11358. We would like to thank M. Tanatar, C. Martin, E. Colombier, E. D. Mun, M. E. Tillman, S. Kim, and X. Lin for help and useful discussions.

[1] Y. Kamihara, T. Watanabe, M. Hirano, and H. Hosono, J. Am. Chem. Soc. **130**, 3296 (2008).
[2] M. Rotter, M. Tegel, and D. Johrendt, Phys. Rev. Lett. **101**, 107006 (2008).
[3] Z.-A. Ren, W. Lu, J. Yang, W. Yi, X.-L. Shen, Zheng-Cai, G.-C. Che, X.-L. Dong, L.-L. Sun, F. Zhou, and Z.-X. Zhao, Chin. Phys. Lett. **25**, 2215 (2008).
[4] A. S. Sefat, R. Jin, M. A. McGuire, B. C. Sales, D. J. Singh, and D. Mandrus, Phys. Rev. Lett. **101**, 117004 (2008).
[5] L. J. Li, Y. K. Luo, Q. B. Wang, H. Chen, Z. Ren, Q. Tao, Y. K. Li, X. Lin, M. He, Z. W. Zhu, G. H. Cao, and Z. A. Xu, New J. Phys. **11**, 025008 (2009).
[6] A. S. Sefat, A. Huq, M. A. McGuire, R. Jin, B. C. Sales, D. Mandrus, L. M. D. Cranswick, P. W. Stephens, and K. H. Stone, Phys. Rev. B **78**, 104505 (2008).
[7] S. Paulraj, Shilpam Sharma, A. Bharathi, A. T. Satya, Sharat Chandra, Y. Hariharan, and C. S. Sundar, arXiv:0902.2728 (unpublished).
[8] F. Han, X. Zhu, P. Cheng, B. Shen, and H.-H. Wen, arXiv:0903.1028 (unpublished).
[9] X. Zhu, H. P. C. Fei, B. Shen, and H.-H. Wen, arXiv:0903.0323 (unpublished).
[10] F. Han, X. Zhu, Y. Jia, L. Fang, P. Cheng, H. Luo, B. Shen, and H.-H. Wen, arXiv:0902.3957 (unpublished).
[11] N. Ni, M. E. Tillman, J.-Q. Yan, A. Kracher, S. T. Hannahs, S. L. Bud'ko, and P. C. Canfield, Phys. Rev. B **78**, 214515 (2008).
[12] J.-H. Chu, J. G. Analytis, C. Kucharczyk, and I. R. Fisher, Phys. Rev. B **79**, 014506 (2009).
[13] F. L. Ning, K. Ahilan, T. Imai, A. S. Sefat, R. Jin, M. A. McGuire, B. C. Sales, and D. Mandrus, J. Phys. Soc. Jpn. **78**, 013711 (2009).
[14] L. Fang, H. Luo, P. Cheng, Z. Wang, Y. Jia, G. Mu, B. Shen, I. I. Mazin, Lei Shan, Cong Ren, and Hai-Hu Wen, arXiv:0903.2418 (unpublished).
[15] C. Lester, J.-H. Chu, J. G. Analytis, S. C. Capelli, A. S. Erickson, C. L. Condron, M. F. Toney, I. R. Fisher, and S. M. Hayden, Phys. Rev. B **79**, 144523 (2009).
[16] D. K. Pratt, W. Tian, A. Kreyssig, J. L. Zarestky, S. Nandi, N. Ni, S. L. Bud'ko, P. C. Canfield, A. I. Goldman, and R. J. McQueeney, arXiv:0903.2833, Phys. Rev. Lett. (to be published).
[17] P. C. Canfield, S. L. Bud'ko, N. Ni, J. Q. Yan, and A. Kracher, arXiv:0904.3134 (unpublished).
[18] P. C. Canfield and Z. Fisk, Philos. Mag. B **65**, 1117 (1992).
[19] M. A. Tanatar, N. Ni, C. Martin, R. T. Gordon, H. Kim, V. G.

Kogan, G. D. Samolyuk, S. L. Bud'ko, P. C. Canfield, and R. Prozorov, Phys. Rev. B **79**, 094507 (2009).
[20] M. A. Tanatar, N. Ni, G. D. Samolyuk, S. L. Bud'ko, P. C. Canfield, and R. Prozorov, Phys. Rev. B **79**, 134528 (2009).
[21] M. Rotter, M. Tegel, D. Johrendt, I. Schellenberg, W. Hermes, and R. Pöttgen, Phys. Rev. B **78**, 020503(R) (2008).
[22] S. L. Bud'ko, N. Ni, S. Nandi, G. M. Schmiedeshoff, and P. C. Canfield, Phys. Rev. B **79**, 054525(R) (2009).
[23] S. R. Saha, N. P. Butch, K. Kirshenbaum, and Johnpierre Paglione, Phys. Rev. B **79**, 224519 (2009).
[24] E. Colombier, S. L. Bud'ko, N. Ni, and P. C. Canfield, Phys. Rev. B **79**, 224518 (2009).
[25] Marianne Rotter, Michael Pangerl, Marcus Tegel, and Dirk Johrendt, Angew. Chem. Int. Ed. **47**, 7949 (2008).
[26] S. Jiang, C. Wang, Z. Ren, Y. Luo, G. Cao, and X. Zhu'an, arXiv:0901.3227 (unpublished).